

This is an Open Access document downloaded from ORCA, Cardiff University's institutional repository: <https://orca.cardiff.ac.uk/id/eprint/181751/>

This is the author's version of a work that was submitted to / accepted for publication.

Citation for final published version:

Zhang, Haobo, Xiang, Wang, Wang, Yining, Xu, Yan and Wen, Jinyu 2025. Hierarchical energy control of MMC-MTDC system integrated with offshore wind farms for optimal frequency support provision. IEEE Transactions on Power Delivery 40 (6) , pp. 3672-3683. 10.1109/TPWRD.2025.3622732

Publishers page: <http://dx.doi.org/10.1109/TPWRD.2025.3622732>

Please note:

Changes made as a result of publishing processes such as copy-editing, formatting and page numbers may not be reflected in this version. For the definitive version of this publication, please refer to the published source. You are advised to consult the publisher's version if you wish to cite this paper.

This version is being made available in accordance with publisher policies. See <http://orca.cf.ac.uk/policies.html> for usage policies. Copyright and moral rights for publications made available in ORCA are retained by the copyright holders.



# Hierarchical Energy Control of MMC-MTDC System Integrated with Offshore Wind Farms for Optimal Frequency Support Provision

Haobo Zhang, Wang Xiang, *Senior Member, IEEE*, Yining Wang, Yan Xu, *Senior Member, IEEE*, Jinyu Wen, *Senior Member, IEEE*

**Abstract**—This paper proposes an energy coordination control scheme for offshore wind farms (OWFs) integrated modular multilevel converter-based multi-terminal direct current (MMC-MTDC) system towards enhanced grid frequency support. First, a two-layer hierarchical energy control framework is established. At the lower layer, a local energy coordination controller is designed to directly regulate OWF rotor kinetic energy and MMC capacitor energy by using local measurements, eliminating energy utilization errors. At the upper layer, an energy optimization method is developed to dispatch multiple energy for achieving optimal energy utilization and minimizing grid frequency deviations. In addition, a multi-stage energy recovery strategy is designed, ensuring frequency stability during the recovery process and enabling the OWFs-MTDC system to support multiple successive frequency events. Finally, the effectiveness and robustness of the proposed method are verified in a test system jointly built in PSCAD/EMTDC and MATLAB.

**Index Terms**—Offshore wind, modular multilevel converter, energy coordination, frequency support, model predictive control.

## I. INTRODUCTION

With the increasing integration of offshore wind farms into modern power grids, the MMC-MTDC system is emerging as a flexible solution for large-scale OWF integration into onshore AC systems. However, due to the reduced grid inertia, the OWFs-MTDC system is also expected to provide frequency support to the connected power grids [1]-[3].

Considering the need for high power generation efficiency, OWFs do not work under deloading operation conditions, resulting in no power reserve in the system [4]. In this scenario, energy reserves such as the kinetic energy of OWFs and the capacitor energy in the MTDC system can be leveraged to participate in grid frequency response. References [5]-[7] proposed a coordinated control method between kinetic energy and capacitor energy using a dual droop control ( $f_g-V_{dc}-f_{off}$ ). This method adjusts the DC link voltage ( $V_{dc}$ ) to link changes in onshore grid frequency ( $f_g$ ) to offshore frequency shifts ( $f_{off}$ ), enabling MTDC systems to utilize capacitor energy and OWFs

This work was supported in part by the National Key Research and Development Program of China (No. 2022YFB2405400) and in part by the National Natural Science Foundation of China (No. 52237004). (Corresponding author: *Wang Xiang*).

Haobo Zhang, Wang Xiang, Yining Wang and Jinyu Wen are with the School of Electrical and Electronic Engineering, Huazhong University of Science and Technology, 430074, Wuhan, China, and also with the State Key Laboratory of Advanced Electromagnetic Technology, Huazhong University of Science and Technology, 430074, Wuhan, China (e-mail: zhanghaobo9902@foxmail.com; xiangwang1003@hust.edu.cn; wangyining0712@foxmail.com; jinyu.wen@hust.edu.cn).

Yan Xu is with the School of Electrical and Electronic Engineering, Nanyang Technological University, 639798, Singapore (xuyan@ntu.edu.sg).

to release rotor kinetic energy for frequency regulation.

To utilize the kinetic energy in OWFs, the frequency-power ( $f_g-P$ ) droop control and the virtual inertia ( $df_g/dt-P$ ) control have been added to the MPPT controller to change output power during frequency variation [8][9]. [10] proposed a preset power based droop control scheme, which can effectively improve the frequency response performance. Referring to grid code regulations, reference [11] further designed rotor speed-power ( $\omega_m-P$ ) control. However, since the setpoint power of MPPT is the cube of the rotor speed, rotor speed deviation from the initial point will cause a counter-effect of the MPPT controller, leading to the OWF support power being less than the desired power [12]. Consequently, the rotor kinetic energy may not be fully utilized, diminishing the frequency support.

For capacitor energy utilization in MTDC systems, the aforementioned references regulated the DC link voltage to use the MMC capacitor energy. Nevertheless, as pointed out in [13], a narrow range of DC link voltage variation can limit capacitor energy utilization, thereby reducing the effectiveness of frequency support. To enhance the efficiency of MTDC capacitor energy utilization, references [14] and [15] developed several frequency-energy droop control schemes that directly regulate capacitor energy for frequency support. Nonetheless, these methods did not consider coordination with OWF kinetic energy, and their effectiveness depends on the actual system frequency. If the energy utilization reaches its limits during certain grid frequency events, the MTDC system may abruptly stop providing support, leading to further frequency drops [16].

In addition to the limitations in energy utilization, it is important to note that the energy coordination methods for OWFs-MTDC systems discussed above rely on traditional droop and proportional-integral (PI) controllers. Specifying constant control gains prevents the system from offering maximum frequency support in various grid disturbances, such as AC load disturbances, wind speed changes, etc. Although different adaptive control methods [16] and [17] are respectively introduced to optimize MMC capacitor energy utilization and OWF kinetic energy utilization for improving grid frequency regulation, various constraints cannot be dealt with simultaneously with classic PI controllers, e.g., power, DC voltage and energy limits in OWFs-MTDC systems.

To achieve optimal frequency response, online optimization techniques are typically applied in frequency support control while accounting for various constraints. For OWFs-MTDC systems, various types of model predictive control (MPC)-based frequency support control schemes have been studied, including centralized MPC [18], mixed centralized/

decentralized MPC [19], and distributed MPC [20]-[24]. However, these methods primarily focus on power coordination and depend on the availability of power reserves in deloaded OWFs and asynchronous grids. For instance, reference [18] designed a centralized MPC controller to coordinate the operations of synchronous generators (SGs) and the deloaded OWFs, minimizing frequency deviations in each grid. References [19]-[24] implemented independent MPC controllers at each converter to regulate the output power of MMCs for optimal frequency regulation separately. Nevertheless, these studies assumed that sufficient power sources were available in the test systems.

In scenarios without power reserves, reference [25] explored the optimal utilization of wind farms' kinetic energy for frequency regulation using nonlinear MPC. On this basis, references [26] and [27] examined the MPC-based energy coordination between OWFs and battery storage systems, as well as between OWFs and offshore DC collection grid capacitors. However, the optimal coordination between OWF kinetic energy and MMC capacitor energy in the OWFs-MTDC system has not yet been investigated. Therefore, key challenges that need to be addressed include 1) how to flexibly regulate these two types of energy; 2) how to optimize their utilization to enhance frequency support. Additionally, the energy recovery after frequency support should be considered.

Therefore, a two-layer hierarchical energy control framework is developed for the OWFs-MTDC system to efficiently coordinate the utilization of OWF kinetic energy and MMC capacitor energy for enhancing frequency support. The main novelty and contributions of this paper are listed:

- A local energy coordination control scheme is devised as the lower-layer controller. This scheme directly regulates multiple energy sources by incorporating rotor speed control of OWFs and active energy control of MMCs. Unlike conventional coordinated control, this approach mitigates the problem of insufficient energy utilization.
- A distributed MPC-based energy utilization method is proposed as the upper-layer controller to dispatch OWF kinetic energy and MMC capacitor energy, ensuring enhanced frequency response and smooth energy recovery with less communication dependence.

This paper is organized as follows. Section II describes the test system and the equivalent frequency response model. Section III analyzes the limitations of the conventional energy coordination scheme. Section IV proposes a hierarchical energy control framework of the OWFs-MTDC system, including the designed energy coordination control and distributed MPC-based energy utilization method, also considering energy recovery. The effectiveness and robustness of the proposed method are verified by simulations in Section V. Finally, conclusions are drawn in Section VI.

## II. SYSTEM DESCRIPTION AND MODELING

### A. System Description

Fig. 1 illustrates the investigated four-terminal MMC-HVDC system integrating with OWFs. OWF1 and OWF2 are the same

OWFs in different regions, and the capacity is 1100MW. The mechanical parameters of the wind turbine are according to the GE benchmark model, as listed in Table A I [28]. In the MTDC system, master-slave control is adopted. MMC1 and MMC3 are the DC voltage station and power station, respectively. MMC2 and MMC4 are AC voltage stations. And all MMCs adopt half-bridge sub-modules (SMs). The detailed parameters of MMC stations are shown in Table A II. In this work, the SM capacitance is designed following the practical projects, with an energy storage time constant of about 40ms.

The topology and line parameters of the onshore AC grid refer to reference [16]. All SGs are represented by the sub-transient model and equipped with governor control (steam turbine). The basic and control parameters of SGs are listed in Table A III and Table A IV, respectively.

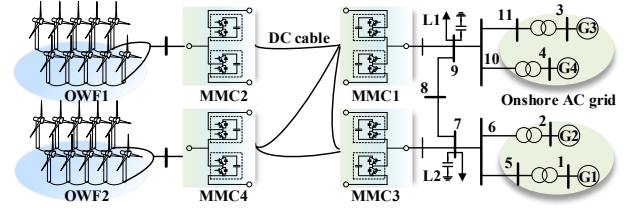


Fig. 1. The investigated OWFs-MTDC system.

### B. System Frequency Response Model

According to SGs' model, the frequency response model of a large AC grid can be obtained by the methods in [29][30], as shown in Fig. 2. Thus, the expression can be derived as [14]:

$$2H_s \Delta \dot{f}_{\text{grid}} = \Delta P_m - \Delta P_L + \Delta P_{WF1} + \Delta P_{WF2} + \Delta P_{MTDC} \quad (1)$$

where the dot “.” above a variable denotes the derivative with respect to time.  $H_s$  is the equivalent inertia constant of the AC grid.  $\Delta P_m$  is the supplementary mechanical power of SGs, offered by the governor and reheat turbine, as shown in the shaded box in Fig. 2. The aggregated gains ( $R$ ,  $K_3$ ,  $K_4$ ,  $K_5$ ) and time constants ( $T_1$ ,  $T_2$ ,  $T_3$ ,  $T_4$ ,  $T_5$ ) are defined in Table A IV.

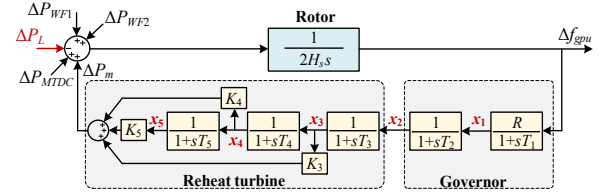


Fig. 2. The aggregated frequency response model of the AC grid.

Besides,  $\Delta P_L$  is the load disturbance power.  $\Delta P_{MTDC}$  denotes the support power using the capacitor energy stored in the MMC-MTDC system.  $\Delta P_{WF_i}$  ( $i=1, 2$ ) denotes the support power provided by the rotor kinetic energy of the  $i$ th OWF, respectively. Notably, the above power is in per-unit value, while the base value is the total capacity of SGs, namely  $S_G$ . Thus, the different support power can be obtained as:

$$\Delta P_{MTDC} = -\frac{W_{C0}}{S_G} \cdot \frac{dW_{Cpu}}{dt} \quad (2)$$

$$\Delta P_{WF_i} = -\frac{E_{k0i}}{S_G} \cdot \frac{dE_{kpu}}{dt} + \frac{\Delta P_{Wmi}}{S_G} \quad (i=1, 2) \quad (3)$$

where subscript “ $i$ ” denotes the variables associated with the  $i$ th OWF.  $W_{Cpu}$  and  $W_{C0}$  are the MTDC capacitor energy in per-unit value and its rated value.  $E_{kpu}$  and  $E_{k0i}$  denote the kinetic energy

in per-unit value and its rated value of the  $i$ th OWF.  $\Delta P_{Wmi}$  is the mechanical power variation of the  $i$ th OWF. Then,  $E_{kpi}$  can also be calculated by rotor speed, that is:

$$E_{kpi} = \omega_{mi}^2 \quad (4)$$

where  $\omega_{mi}$  is the rotor speed of the  $i$ th OWF in per-unit value.

In (3),  $\Delta P_{Wmi}$  is expressed as:

$$\Delta P_{Wmi} = \frac{1}{2} \rho \pi r^2 C_{pi} (\lambda_i (\omega_{mi}, w_{si}), \beta_i) w_{si}^3 - P_{Wm0} \quad (5)$$

where mechanical power variation  $P_{Wm0}$  denotes the mechanical power of the OWF under rated conditions.  $\rho$  is the air density.  $r$  is the radius of the turbine blade.  $w_{si}$  is the wind speed of the  $i$ th OWF.  $C_{pi}$  is the power coefficient for the given pitch angle  $\beta_i$  and the tip-speed ratio  $\lambda_i$ . Considering the overload of OWFs is slight and short-term during frequency support, the pitch angle control can be assumed as inactive, and  $\beta_i$  is regarded as 0.

### III. CONVENTIONAL ENERGY COORDINATION SCHEME

Fig. 3 shows the conventional coordinated frequency control scheme for OWFs-MTDC systems in [4]-[6]. The red arrows show the traditional dual droop ( $f_g - V_{dc} - f_{off}$ ) control applied in onshore and offshore MMCs, which enables OWFs to sense changes in onshore frequency  $f_g$ .

The OWF control is shown in the blue cube in Fig. 3. The support power  $\Delta P_{add}$  is generated by frequency control and added to the MPPT setpoint power. Considering the controller can well track the power reference, the actual support power  $\Delta P_{WF}$  of OWF is expressed as:

$$\Delta P_{WF} = \Delta P_{MPPT} + \Delta P_{add} \quad (6)$$

where  $\Delta P_{MPPT}$  is the variation in the MPPT setpoint.

When the grid frequency decreases, the OWF kinetic energy is released for support. As the rotor speed decreases,  $\Delta P_{MPPT}$  is always minus since  $P_{MPPT}$  is approximately proportional to the cube of the rotor speed. Thus,  $\Delta P_{WF}$  will be less than the desired power  $\Delta P_{add}$ , and the kinetic energy cannot be used effectively.

The control of onshore DC voltage MMC is presented in the green cube in Fig. 3. The MMC control with two modulation ratios ( $M_d$  and  $M_q$ ) is adopted. Since the SM capacitor voltage is proportional to the DC link voltage, the frequency control is

applied to utilize the MMC capacitor energy by regulating the DC link voltage. However, the allowable DC voltage variation is  $\pm 0.2$  p.u., much less than  $[-0.232$  p.u.,  $0.5$  p.u.] of capacitor voltage variation [16]. Hence, the DC voltage-based energy regulation method limits capacitor voltage (energy) utilization.

To sum up, the conventional energy coordination method indirectly regulates energy, with the problem of insufficient energy utilization. Meanwhile, the control coefficients of  $k$ ,  $D$  and  $H$  in frequency control are usually fixed, also making it hard to achieve optimal energy coordination under various scenarios.

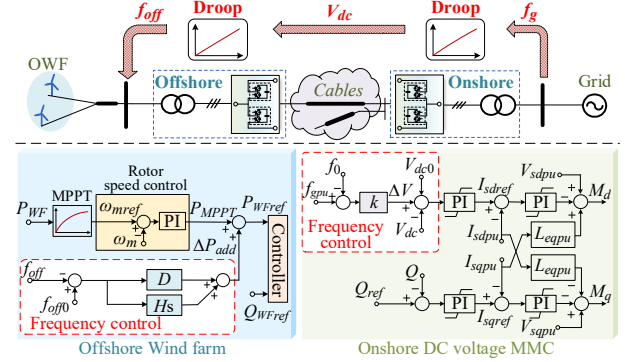


Fig. 3. Conventional coordination control method.

### IV. PROPOSED ENERGY COORDINATION METHOD

#### A. Hierarchical Energy Control Framework

Fig. 4 illustrates the proposed hierarchical energy control framework for efficiently coordinating energy reserves in OWFs and MMCs. The proposed framework consists of lower- and upper-layer controllers. The lower-layer controller aims to directly regulate kinetic and capacitor energy, containing rotor speed control in OWFs and energy control in MMCs, as shown in red cubes in Fig. 4. The upper-layer controller utilizes two types of energy for optimal frequency support, where the distributed MPC controllers, e.g., onshore and offshore MPCs, are designed to generate control references for the lower-layer control, as shown in yellow boxes in Fig. 4. To ensure the generated control references by different MPCs are consistent, MPC controllers in all MMCs are the same.

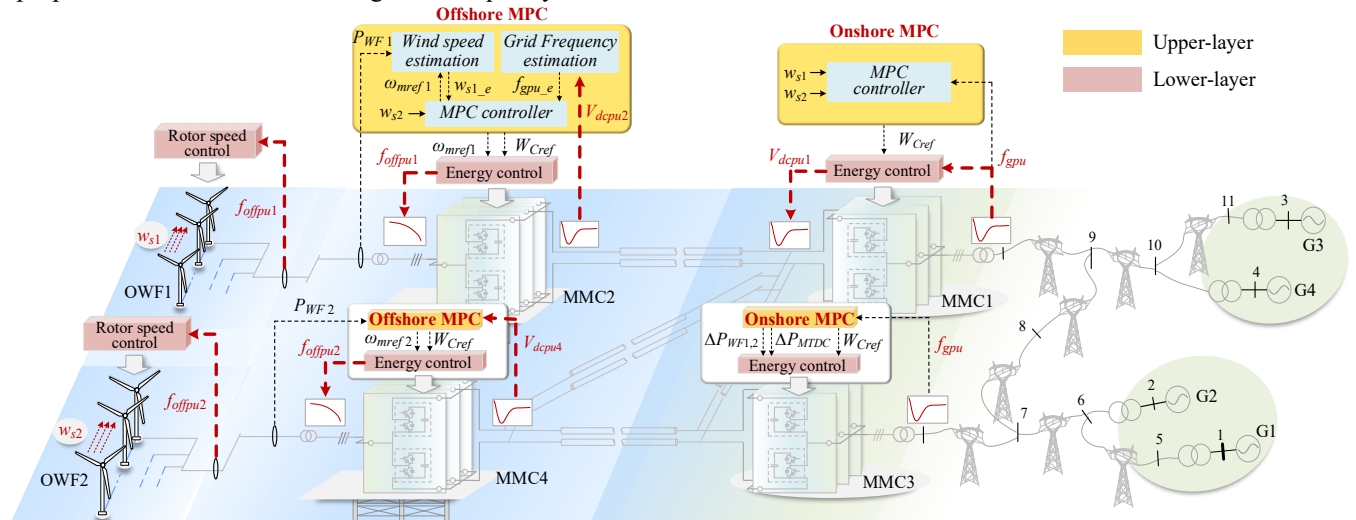


Fig. 4. The proposed hierarchical energy control framework for OWFs-MTDC system.

When implementing MPC controllers, the grid frequency  $f_{gpu}$  and wind speeds of OWFs ( $w_{s1}$  and  $w_{s2}$ ) are required. For onshore MPCs, the grid frequency is measured at the AC side of onshore MMCs. The wind speeds are received by satellite communication.

For the offshore MPC, two estimators are designed to estimate the grid frequency  $f_{gpu,e}$  and the wind speed of the connected OWF (e.g.,  $w_{s1,e}$  and  $w_{s2,e}$ ) using local measurements (DC voltage and OWF output power). Satellite communication is also used to get the other OWF wind speed.

Although satellite communication is involved in the proposed method, the communication volume is much less than the centralized MPC methods. For instance, the common centralized MPC method in [18] requires the communication of mass control references, causing a very high data traffic. In contrast, the distributed method only requires communication of wind speeds. Due to the slow time scale of wind speed changes, there is no need for frequent communication.

### B. Lower-layer Energy Coordination Control Design

Different from the indirect energy coordination control scheme in Fig. 3, a direct energy coordination control strategy is first employed in the lower-layer controller, as follows:

- Regarding the OWFs, the control structure is shown in the blue cube in Fig. 5. Since the kinetic energy is the square of the rotor speed, the rotor speed control is switched from MPPT mode to regulate kinetic energy during frequency response.
- For the MMCs, as shown in the gray cube in Fig. 5, the active energy control structure containing AC modulation ratios ( $M_d$ ,  $M_q$ ), DC modulation ratios ( $M_{dc}$ ) and capacitor voltage modulation ratios ( $M_c$ ) is adopted [13], enabling MMC to regulate the SM capacitor voltage independently. Then, the capacitor energy control of different MMCs is designed, as shown in green blocks in Fig. 5. Regarding the DC voltage station (MMC1), energy control is implemented by AC current control [31]. For other MMCs, energy

regulation is achieved by DC current control.

Then, to achieve energy coordination among all MMCs, the traditional  $f_g$ - $V_{dc}$  droop control in Fig. 3 is introduced in the DC voltage station MMC1, which is expressed as:

$$V_{dcref} = V_{dc0} + k_f (f_{gpu} - f_{g0}) \quad (7)$$

where  $V_{dcref}$  is the DC voltage control reference.  $f_{gpu}$  is the grid frequency in per-unit value. Subscript "0" is used to indicate the rated value. And  $k_f$  is a droop gain. With (7), other MMCs can sense grid frequency changes by measuring DC link voltage, and then regulate capacitor energy synchronously.

Meanwhile, a method of regulating OWF kinetic energy by offshore MMC is developed. Unlike the  $V_{dc}$ - $f_{off}$  droop in Fig. 3, a  $\omega_m$ - $f_{off}$  droop control is designed for offshore MMCs to couple the offshore frequency  $f_{off}$  with the desired OWF rotor speed  $\omega_m$ . The expression of the  $\omega_m$ - $f_{off}$  droop control in offshore MMCs is written as:

$$f_{offref\ i} = f_{off0} + k_\omega (\omega_{mref\ i} - \omega_{m0}) \quad (8)$$

where the subscript "i" denotes the control reference of the MMC integrated with the  $i$ th OWF, respectively.  $f_{offref}$  is the control reference of the frequency control.  $f_{off0}$  and  $\omega_{m0}$  represent the rated values. And  $k_\omega$  is the droop gain.

Then, a coordinated control is advised for the  $i$ th OWFs to generate the rotor speed reference  $\omega_{mref\ i}$  from their own offshore frequency  $f_{off\ i}$ . The expression is obtained by (8):

$$\omega_{mref\ i} = \frac{1}{k_\omega} (f_{off\ pu\ i} - f_{off0}) + \omega_{m0} \quad (9)$$

where  $f_{off\ pu\ i}$  is the offshore frequency measures at the  $i$ th OWF. Thus, the obtained  $\omega_{mref\ i}$  can be imported into the rotor speed control of the  $i$ th OWF, achieving rotor kinetic regulation.

As shown in Fig. 5, MMC3 is the constant power station. If the power of MMC3 remains fixed, the total support power  $\Delta P_{tot}$  ( $=\Delta P_{MTDC} + \Delta P_{WF1} + \Delta P_{WF2}$ ) will flow through the DC voltage station MMC1, causing overload in MMC1. Hence, power-sharing control is proposed for MMC3 to share the total support power, which can be expressed as:

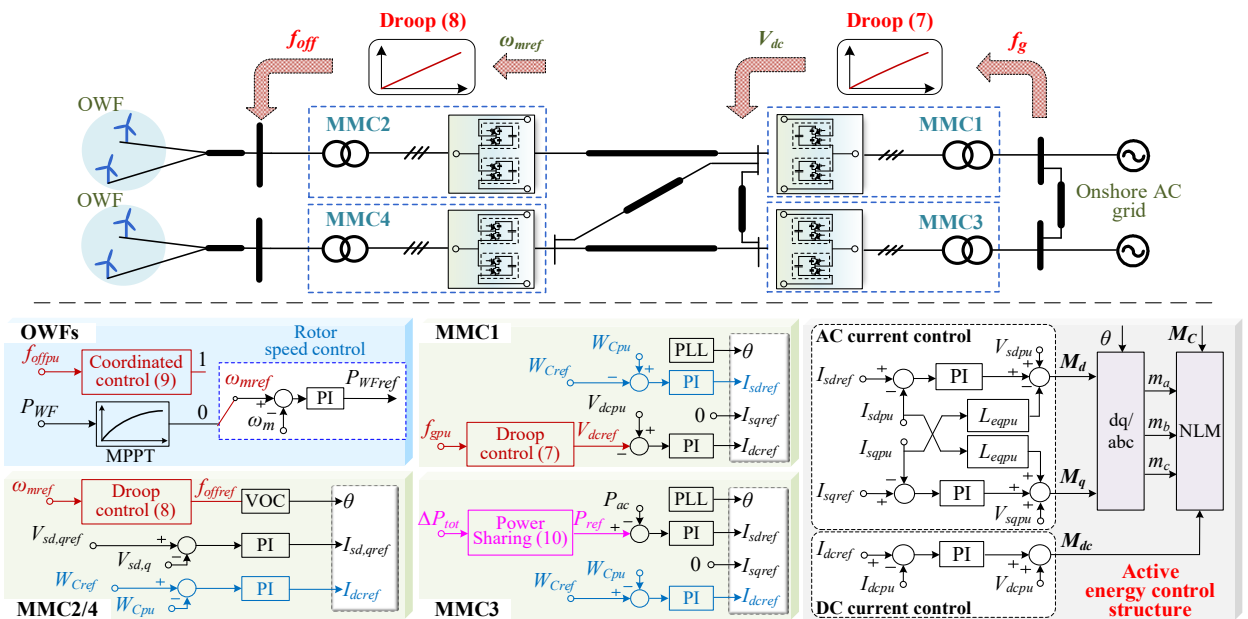


Fig. 5. The proposed energy coordination control structure of the OWFs-MTDC system.

$$P_{ref} = K \cdot \Delta P_{lat} + P_{ref0} \quad (10)$$

where  $P_{ref0}$  is the power control reference under normal conditions.  $K$  is the distribution coefficient.

As analyzed above, all the MMCs and OWFs are connected by local measurements, facilitating flexible regulation of various energies. Meanwhile, the local-based control also decreases the communication pressure of the whole system.

### C. Upper-layer Energy Optimization Control Design

For dynamically optimal frequency response, the MPC controller is a promising solution to coordinate the energy in MMC capacitors and OWF rotors. Since the various types of energy can be represented by corresponding support power, as expressed in (2) and (3), the optimization of energy is equivalent to the optimization of support power in Fig. 2.

Firstly, based on the frequency response model shown in Fig. 2, the state-space equations can be obtained as:

$$\begin{cases} \dot{\mathbf{x}} = \mathbf{A}_0 \mathbf{x} + \mathbf{B}_0 \mathbf{u} + \mathbf{R}_{L0} \mathbf{z} \\ \mathbf{y} = \mathbf{C} \mathbf{x} \end{cases} \quad (11)$$

where state vector  $\mathbf{x} = [\Delta f_{gpu}, x_1, x_2, x_3, x_4, x_5]^T$ . Input vector  $\mathbf{u} = [\Delta P_{WF1}, \Delta P_{WF2}, \Delta P_{MTDC}]^T$ , which are variables required to be optimized. The disturbance vector  $\mathbf{z} = [\Delta P_L]$ . In addition, the output of the system is defined as the grid frequency variation. Thus, the output vector  $\mathbf{y} = [\Delta f_{gpu}]$ .  $\mathbf{A}_0$ ,  $\mathbf{B}_0$ ,  $\mathbf{R}_{L0}$  and  $\mathbf{C}$  are the state matrix, input matrix, disturbance matrix and output matrix, which can be calculated according to Fig. 2.

Using the Zero-Order Hold discretization technique, a discrete-time prediction model can be obtained from (11). It yields,

$$\begin{cases} \mathbf{x}_{k+1} = \underbrace{(\mathbf{I} + T_s \mathbf{A}_0)}_{\mathbf{A}} \mathbf{x}_k + \underbrace{T_s \mathbf{B}_0}_{\mathbf{B}} \mathbf{u}_k + \underbrace{T_s \mathbf{R}_{L0}}_{\mathbf{R}_L} \mathbf{z}_k \\ \mathbf{y}_k = \mathbf{C} \mathbf{x}_k \end{cases} \quad (12)$$

where  $\mathbf{I}$  is the identity matrix.  $T_s$  is the sampling period, and the subscript  $k$  is the time step.  $\mathbf{A}$ ,  $\mathbf{B}$  and  $\mathbf{R}_L$  are discretized state-space matrices.

From (12), we see that solving the MPC problem also requires the load disturbance power  $\Delta P_L$ , which cannot be measured in general. In this paper, the method of moving horizon estimation (MHE) is employed to estimate the state of  $\Delta P_L$ . The details about the MHE are referred to [24]. The prediction model (12) can be modified as:

$$\begin{cases} \begin{bmatrix} \mathbf{x}_{k+1} \\ \mathbf{z}_{k+1} \\ \mathbf{x}'_{k+1} \end{bmatrix} = \begin{bmatrix} \mathbf{A} & \mathbf{R}_L \\ \mathbf{0} & \mathbf{1} \end{bmatrix} \begin{bmatrix} \mathbf{x}_k \\ \mathbf{z}_k \\ \mathbf{x}'_k \end{bmatrix} + \begin{bmatrix} \mathbf{B} \\ \mathbf{0} \end{bmatrix} \mathbf{u}_k + \begin{bmatrix} \mathbf{0} \\ T_s \\ \mathbf{E} \end{bmatrix} \delta_k^L \\ \mathbf{y}_k = \begin{bmatrix} \mathbf{C} & \mathbf{0} \end{bmatrix} \begin{bmatrix} \mathbf{x}_k \\ \mathbf{z}_k \end{bmatrix} + \delta_k^f \end{cases} \quad (13)$$

where  $\mathbf{x}'_k$  is the modified state vector at the  $k$  time step.  $\mathbf{A}'$ ,  $\mathbf{B}'$  and  $\mathbf{C}'$  are the modified matrices. Both  $\delta_k^L$  and  $\delta_k^f$  are independent Gaussian white-noise processes.

Then, based on the prediction model, the cost function has to be specified to obtain the time series of the optimal input vector  $\mathbf{u}$ . For improving the grid's frequency stability, the primary objective of the designed MPC is to suppress the system output  $\mathbf{y}$  (i.e., frequency deviations  $\Delta f_{gpu}$ ). Moreover, to avoid

exceeding the energy utilization limit, magnitudes of the input  $\mathbf{u}$  (i.e., support power  $\Delta P_{WF1}$ ,  $\Delta P_{WF2}$  and  $\Delta P_{MTDC}$ ) should be restricted. Therefore, the cost function is designed as:

$$\min_{\mathbf{u}_k} \mathbf{J} = \sum_{h=0}^{N_p-1} \left( (\mathbf{y}_{k+h} - \mathbf{y}_{ref})^T \mathbf{Q} (\mathbf{y}_{k+h} - \mathbf{y}_{ref}) + \mathbf{u}_{k+h}^T \mathbf{R} \mathbf{u}_{k+h} \right) + (\mathbf{y}_{k+N_p} - \mathbf{y}_{ref})^T \mathbf{F} (\mathbf{y}_{k+N_p} - \mathbf{y}_{ref}) \quad (14)$$

where  $N_p$  is the prediction and control horizon.  $\mathbf{y}_{ref}$  is the desired output reference, which is normally 0 for maximum frequency support.  $\mathbf{Q}$  and  $\mathbf{R}$  are the weighting matrices corresponding to the future predicted frequency deviations and control input signals, respectively. Meanwhile, the  $(\mathbf{y}_{k+N_p} - \mathbf{y}_{ref})$  is the terminal cost.  $\mathbf{F}$  is the corresponding weighting matrix [25].

Finally, considering the limits of OWF rotor speed and MMC capacitor energy, the constraints on the control input vector  $\mathbf{u}$  can be designed.

1) *Constraints on OWF support power:* As presented in [32], the OWF rotor speed must be within a safe range. Combining and discretizing (3)-(5), the relationship between support power  $\Delta P_{WFi}$  and rotor speed  $\omega_{mi}$  can be calculated as ( $i=1,2$ ):

$$\begin{aligned} \frac{\Delta P_{WFi}(k)}{u_k(i)} = & -\frac{2E_{k0}}{S_G T_s} \omega_{mi}(k) [\omega_{mi}(k) - \omega_{mi}(k-1)] \\ & + \frac{\rho \pi r^2 w_{st}^3}{2S_G} [C_{pi}(\omega_{mi}(k), w_{st}) - C_{p0i}] \end{aligned} \quad (15)$$

where  $u_k(i)$  is the  $i$ th element of the input vector  $\mathbf{u}$  at the  $k$ th time step.  $C_{p0i}$  is the nominal power coefficient, which can be determined by the initial rotor and wind speed. Considering the rotor speed limits of  $\omega_m^{lim} = [\omega_m^{min}, \omega_m^{max}]$ , the constraints on the OWF support power can be obtained as [27]:

$$\mathbf{u}^{min}(i) \Big|_{\omega_{mi}(k)=\omega_m^{max}} \leq \mathbf{u}_k(i) \leq \mathbf{u}^{max}(i) \Big|_{\omega_{mi}(k)=\omega_m^{min}} \quad (i=1,2) \quad (16)$$

2) *Constraints on MTDC support power:* according to (2), the discrete equation of MTDC support power can be written as:

$$\frac{\Delta P_{MTDC}(k)}{u_k(3)} = -\frac{W_{C0}}{S_G T_s} [W_{Cpu}(k) - W_{Cpu}(k-1)] \quad (17)$$

Considering the MMC capacitor energy limit of  $W_c^{lim} = [W_c^{min}, W_c^{max}]$ , the constraints can be yielded:

$$\mathbf{u}^{min}(3) \Big|_{W_{Cpu}(k)=W_c^{max}} \leq \mathbf{u}_k(3) \leq \mathbf{u}^{max}(3) \Big|_{W_{Cpu}(k)=W_c^{min}} \quad (18)$$

Combining the prediction model (13), cost function (14), constraints (16) and (18), time series of the optimal support power output ( $\Delta P_{WF1}$ ,  $\Delta P_{WF2}$ , and  $\Delta P_{MTDC}$ ) can be obtained. On this basis, the time series of OWFs rotor speed  $\omega_{mi}(k)$  and MMC capacitor energy  $W_{Cpu}(k)$  can be further calculated from (15) and (17), using the MPC power outputs together with the previous-step state variables ( $k-1$ ). Then, they are used as the control references of the lower-layer energy control (i.e.,  $\omega_{mref1}$ ,  $\omega_{mref2}$  and  $W_{cref}$ ). Notably, the wind speed  $w_{st}$  should be known when calculating  $\omega_{mrefi}$  by (15). Thus, communication is adopted in MMCs to receive wind speed information.

Moreover, as presented in Fig. 4, the estimations of the connected OWF wind speed and onshore grid frequency are required for offshore MMCs to implement the proposed MPC controller. Due to the relationship between the DC link voltage and grid frequency in (7), the grid frequency can be estimated

by detecting the local DC voltage. The details of the frequency estimation can be found in [9].

In addition, the relationship between the connected OWF support power  $\Delta P_{WFi}$ , rotor speed  $\omega_{mi}$  and wind speed  $w_{si}$  satisfies the equation (15). Where the  $\Delta P_{WFi}$  can be directly measured. Assuming the rotor speed control can accurately track control references, the  $\omega_{mi}$  can be regarded as the  $\omega_{mrefi}$  generated by offshore MPC controllers. As a result, the wind speed can be estimated by solving (15).

To better illustrate the operating mechanism of the upper-layer MPC controller in different MMCs, Fig. 4 is expanded and detailed as Fig. 6. As shown, all MMCs adopt the same MPC controller, as the required information and outputs are consistent across controllers, as shown in the gray boxes in Fig. 6. The required information includes wind speeds from OWFs ( $w_{s1}$ ,  $w_{s2}$ ) and the grid frequency  $f_{gpu}$ . Moreover, the outputs of the MPCs consist of the desired supporting power from OWFs and MMCs:  $\Delta P_{WF1}$ ,  $\Delta P_{WF2}$ , and  $\Delta P_{MTDC}$ .

The differences lie in the source of the input information and the utilization of the output signals for each MMC. Taking onshore MMC3 for example, both wind speeds of OWF1 and OWF2 are obtained via communication, while the grid frequency is measured locally. The MPC outputs are used for power-sharing control (equation (10)) and for generating the lower-layer capacitor energy control reference  $W_{Cref}$  through equation (17). For offshore MMC2, only the wind speed  $w_{s2}$  of the non-directly connected OWF2 needs to be obtained via communication; all other required information can be derived through local estimators (e.g.,  $w_{s1_e}$  and  $f_{gpu_e}$ ). Moreover, the output  $\Delta P_{WF1}$ , combined with the estimated  $w_{s1_e}$ , is converted into the rotor speed control reference  $\omega_{mref1}$  by equation (15). The third output  $\Delta P_{MTDC}$  is used to generate  $W_{Cref}$  by (17). The control references generated in MMC4 follows a similar principle to that of MMC2.

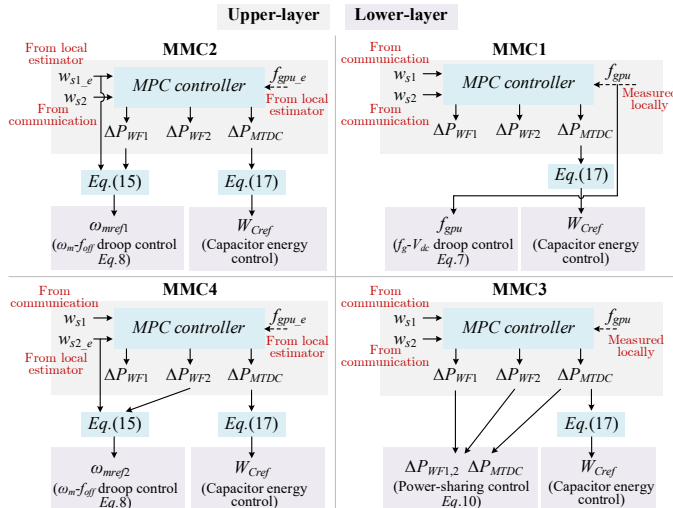


Fig. 6. Diagram of the implementation of MPC controllers in different MMCs.

## D. Energy Recovery Strategy

As analyzed above, the MPC output reference  $y_{ref}$  (frequency deviation  $\Delta f_{gpu}$ ) is set to 0, which can utilize energy to minimize frequency deviation as much as possible. However, during the primary frequency regulation period, there will be a steady state frequency deviation  $\Delta f_{steady}$ . Therefore, consistently setting the

$y_{ref}$  to 0 may lead to energy overutilization, which is not conducive to energy recovery. Regarding this issue,  $y_{ref}$  is designed to change from 0 to  $\Delta f_{steady}$ , that is:

$$y_{ref} = \begin{cases} 0 & , t \leq t_{nadir} \\ \Delta f_{steady} \cdot \min\{k_{re}(t - t_{nadir}), 1\} & , t > t_{nadir} \end{cases} \quad (19)$$

where  $t_{nadir}$  is the time at the frequency nadir, which can be determined by monitoring the rate of change of frequency (RoCoF). And  $k_{re}$  is the change slope of  $y_{ref}$ , here is 0.5. Therefore, the output reference  $y_{ref}$  will be adjusted to  $\Delta f_{steady}$  after 2s. According to Fig. 2, the  $\Delta f_{steady}$  can be calculated by letting  $s=0$  in the governor and reheat turbine loops, yielding:

$$\Delta f_{steady} = \frac{\Delta P_L}{R} \quad (20)$$

In addition, to avoid serious second frequency dips during energy recovery, a multi-stage recovery strategy is developed. Taking the load increase as an example, the proposed energy recovery strategy after energy utilization is depicted in Fig. 7. Defining the disturbance occurrence time as 0, the strategy consists of four stages, as outlined below.

- Stage I ( $t_1$ - $t_2$  after disturbances):** The energy recovery strategy is enabled at  $t_1$  after the disturbance. Within this stage, the rotor speeds of all the OWFs remain unchanged. And the capacitor energy is still utilized to suppress frequency variation.
- Stage II ( $t_2$ - $t_3$  after disturbances):** Considering the frequency deviation is still quite large during this stage, the OWF with a smaller rotor speed deviation is controlled to restore linearly. Meanwhile, the capacitor energy utilization for frequency support is still in operation.
- Stage III and IV ( $t_3$ - $t_4$  and  $t_4$ - $t_5$  after disturbances):** During stage III, the other OWF recovers rotor speed linearly. In stage IV, MMC capacitor energy is restored to its rated value following a quadratic curve, with the slope set to 0 at  $t_5$  for smooth recovery.

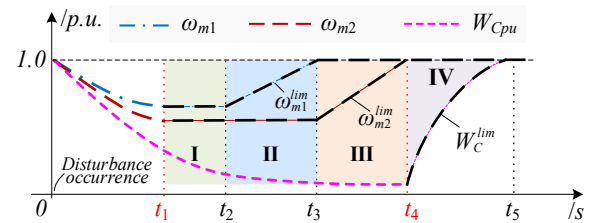


Fig. 7. Illustration of the multi-stage energy recovery method.

To achieve the coordinated recovery of rotor kinetic energy and capacitor energy at the above stages, the distributed MPC controllers are also utilized. By changing the limits in constraints (16) and (18) along the preset black dotted curves in Fig. 7, the desired control references can be generated to realize the sequential energy recovery. It should be noted that limit changes are only carried out during energy recovery periods.

## V. SIMULATION TESTS

To verify the effectiveness of the proposed method, the electromagnetic transient model of the OWFs-MTDC system in Fig. 1 is built in PSCAD/EMTDC. Details of the tested system parameters are presented in the Appendix. The designed MPC

algorithm is implemented on the MATLAB platform. In the PSCAD platform, the simulation time step is set to 50 $\mu$ s. To not affect simulation speed, the frequency of calling the MPC algorithm is selected to 100Hz. Thereby, the sampling period  $T_s$  of the MPC controller is set to 10ms in MATLAB. Meanwhile, the prediction and control horizon  $N_p$  is set to 20, i.e., 200ms.

Considering the energy recovery strategy, rotor speed and capacitor energy limits of the proposed method can be concluded in Table I. Referring to [32], the normal range of the rotor speed is [0.7p.u., 1.2p.u.]. For the MMC capacitor energy, our previous work [16] points out that its lower limit depends on the DC voltage, and the normal range is  $[(0.5V_{dcpu}+0.368)^2, 2.25]$  in per-unit value. During the energy recovery stages, the limits are switched to the corresponding curves shown in Fig. 7.

TABLE I  
LIMITS FOR THE PROPOSED MPC CONTROLLERS

Limits	Normal ranges	Energy recovery period
WF1 rotor speed $\omega_{m1}^{lim}/p.u.$	[0.7, 1.2]	Curves of stage I to IV in Fig. 7
WF2 rotor speed $\omega_{m2}^{lim}/p.u.$		
Capacitor energy $W_c^{lim}/p.u.$	$[(0.5V_{dcpu}+0.368)^2, 2.25]$	Curve in stage IV in Fig. 7

## A. Parameter Settings

### 1) Control parameters:

The control parameters ( $k_\omega$ ,  $k_f$  and  $K$ ) should be determined to implement the proposed local energy coordination control. For the  $f_g$ - $V_{dc}$  droop control of MMC1, the droop gain  $k_f$  is designed by considering the DC voltage and frequency deviation limit. As stated in [33], the statutory limits  $\Delta f_{lim}$  in most countries are  $\pm 0.01p.u.$  with a nominal frequency of 50Hz. Meanwhile, the DC voltage variation limit  $\Delta V_{dclim}$  is  $\pm 0.2p.u.$  [16]. To ensure the DC voltage is within the allowable range at maximum frequency variation,  $k_f$  should satisfy:

$$k_f \leq \frac{\Delta V_{dclim}}{\Delta f_{lim}} = 20 \quad (21)$$

As shown in Table I, the larger the DC voltage drops, the lower the capacitor energy limit. Thus,  $k_f$  is set to 20 for a large capacitor utilization margin.

Regarding the gain  $k_\omega$  in the  $\omega_{mref}$ - $f_{off}$  droop control of offshore MMCs, the limits of the WF rotor speed and offshore frequency are considered. Since the offshore frequency has a wide range of variations,  $k_\omega$  is set to 1.

Moreover, the distribution coefficient  $K$  is determined as:

$$K = \frac{S_{MMC3}}{S_{MMC1} + S_{MMC3}} = 0.364 \quad (22)$$

where  $S_{MMC1}$  and  $S_{MMC3}$  are the rated capacities of MMC1 and MMC3, respectively. Therefore, the support power flowing through MMC1 and MMC3 can be proportional to their capacity without the risk of overload.

### 2) Time points:

Additionally, the time points for energy recovery need to be determined in Fig. 7. Considering the primary frequency response is within 20 seconds [34], the total recovery time  $t_5$  is set to 20s to enable rapid recovery in response to successive system disturbances. Since the critical first swing of a frequency drop/rise lasts about 2-5 seconds [32], the OWFs can stop utilizing kinetic energy after 5 seconds to avoid a severe

second frequency dip during recovery. Therefore,  $t_1$  is set to 5s. The rotor speeds are held constant for an additional 3 seconds, with  $t_2$  set to 8s. This allows the system to stabilize and ensures that the frequency deviation is sufficiently regulated before energy recovery. Finally, the energy recovery time for each component (OWF1, OWF2, and the MTDC system) is evenly divided into three parts for a total of the remaining 12 s.

### 3) Weighting matrices:

The control roles and tuning impacts of MPC parameters (i.e., weighting matrices) are summarized in Table II. As shown, parameter selection involves a trade-off between improving the frequency nadir and mitigating the second frequency dip. Therefore, the parameters should be chosen through a reasonable trade-off and iterative testing process. Specifically, set  $Q=2$ ,  $R=diag(0.1, 0.1, 0.2)$ , and  $F=50$ . Although the weighting matrices in the cost function (14) can be further optimized for better frequency support, the focus of this paper is to validate the capability of the proposed hierarchical energy control framework in fully utilizing multiple energy. Parameter optimization can be further explored in future research.

TABLE II  
IMPACT OF MPC PARAMETERS ON FREQUENCY RESPONSE

MPC Parameter	Control Role	Tuning Impact
$Q$ (scalar)	Penalizes frequency deviation $\Delta f_{gpu}$	Larger $Q$ : improves frequency nadir; may worsen second frequency dip
$R=diag(R_{11}, R_{22}, R_{33})$	Penalizes supporting power of OWF1&2, and MTDC system	Larger $R_{ii}$ : mitigates second frequency dip; may reduce frequency nadir
$F$ (scalar)	Penalizes terminal prediction state	Larger $F$ : improves frequency nadir; may worsen second frequency dip

## B. Validations of the Proposed Method

### 1) Performance of the estimators:

To test the correctness of the designed estimators, some simulation cases are carried out below.

- **Case 1:** a 160MW load increase ( $\Delta P_L=5\%$ ) is applied at bus 7, with wind speeds of OWF1 and OWF2 being 10.8m/s.
- **Case 2:** an 80MW load decrease ( $\Delta P_L=-2.5\%$ ) is applied at bus 7, with wind speeds of 9.0 m/s and 9.8 m/s for OWF1 and OWF2, respectively.

It should be pointed out that the proposed energy recovery control is not activated in these cases. The simulation results are shown in Fig. 8. Fig. 8 (a), (c) and (e) depict the estimated frequency, load disturbance power and wind speed under case 1. In Fig. 8 (a), the grid frequency measured by MMC1 and the estimated frequency by MMC2 and MMC4 are almost coincidental, demonstrating the frequency estimat in offshore MMCs is precise. In Fig. 8 (c), the load disturbance powers estimated by all the MMCs are about 0.05p.u., corresponding to the preset conditions. Although there will be some prediction error in the early period after the disturbance occurs, it will be corrected to the exact value within 2s. Hence, the correctness of load disturbance estimator in (13) is verified. Moreover, the wind speeds of OWF1 and OWF2 can also be correctly estimated at about 10.8m/s, as shown in Fig. 8 (e).

Regarding case 2, the estimated results are presented in Fig. 8 (b), (d) and (f). The frequency estimations in offshore MMCs are also accurate. The estimated load disturbance power is -

0.025p.u., in accord with the actual load disturbance. In addition, the wind speeds of the two OWFs are also accurately estimated, which are 9.0m/s and 9.8m/s, respectively.

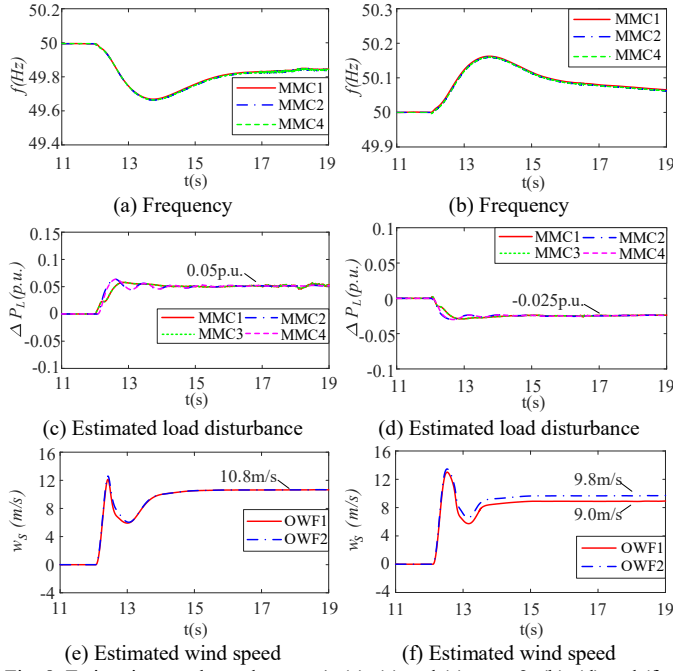


Fig. 8. Estimation results under case 1: (a), (c) and (e); case 2: (b), (d) and (f).

## 2) Performance of the proposed distributed MPC method:

To verify the effectiveness of the proposed distributed MPC-based energy coordination method, a 160MW load increase ( $\Delta P_L=5.0\%$ ) is applied in bus 7, with the wind speeds of OWF1 and OWF2 being 10.8m/s. Meanwhile, to highlight the merits of the proposed method, three different control schemes are compared in the following simulations, they are:

- **D-MPC** (method in this paper): The proposed distributed MPC-based energy utilization method.
- **C-MPC**: The proposed energy utilization method using the centralized MPC (all MMCS and OWFs are controlled by one main MPC controller).
- **D-MPC-noMMC**: The proposed energy utilization and recovery strategies with the designed distributed MPC, considering only OWF rotor kinetic energy as [25].
- **D-MPC-noRotor**: The proposed energy utilization and recovery strategies with the designed distributed MPC, considering only the MMC capacitor energy.

Fig. 9 compares the frequency response using various control schemes. As shown in the red and blue curves, the frequency response using the *D-MPC* is almost the same as *C-MPC*. Thus, the proposed distributed method can effectively provide frequency support even with additional processes of measurement and estimation. Compared to the *D-MPC-noMMC* method, the proposed *D-MPC* method improves the frequency nadir by 8%, verifying the enhanced effect by coordinating MMC energy. Meanwhile, the proposed *D-MPC* method improves the frequency nadir by 27% than the *D-MPC-noRotor* method, demonstrating the enhanced effectiveness of utilizing the rotor kinetic energy of OWFs. Additionally, although the frequency drops many times due to the energy recovery, the maximum frequency drop does not exceed

frequency nadir. Thereby, the properness of the energy recovery strategy is verified.

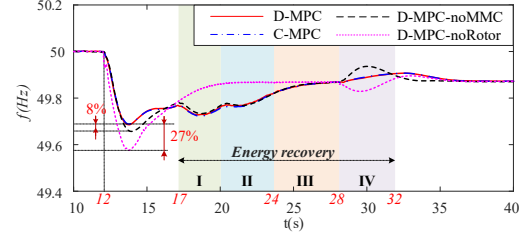


Fig. 9. Comparison of the frequency responses using different methods.

Fig. 10 depicts the control performance using the *D-MPC* method. Fig. 10 (a) and (b) show the control references generated by onshore MPC (e.g., MMC1) and offshore MPC (e.g., MMC4), respectively. As can be seen, different MPCs operate in coordination, ensuring the generated control references are consistent. Meanwhile, the control references match the preset curves in Fig. 7 very well. At 17s, both the OWF1 and OWF2 stop reducing their rotor speed and recover rotor speed linearly at 20s and 24s, respectively. Then, MMCs start to recover capacitor energy with a quadratic curve at 28s.

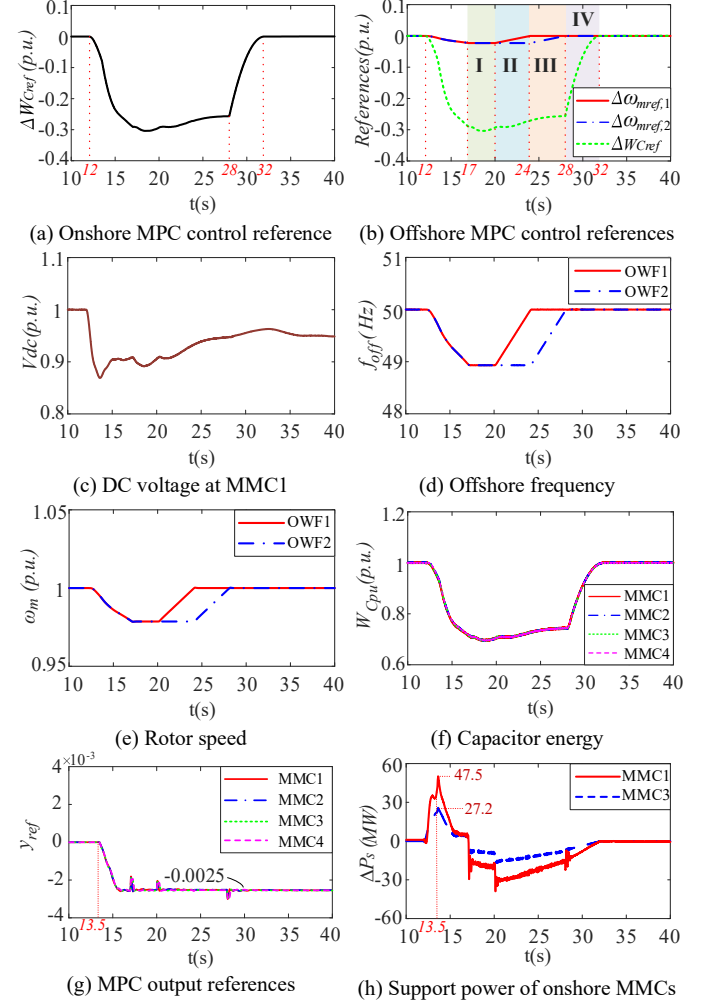


Fig. 10. Performance of the proposed method under a 160MW load increase.

Fig. 10 (c) and (d) show the DC voltage at MMC1 and offshore frequency at the AC side of the two OWFs. The DC voltage changes with the grid frequency variation, and the offshore frequency follows the rotor speed references generated

by offshore MPC. Thus, the dual droop control in the proposed local energy control performs well for energy coordination. The actual rotor speed and MMC energy are presented in Fig. 10 (e) and (f), which can track the control references precisely. Meanwhile, the capacitor energy in all MMCs can be utilized synchronously.

Fig. 10 (g) depicts the MPC output reference  $y_{ref}$  in different MMCs. It can be observed that  $y_{ref}$  changes at 13.5s, from 0 to  $\Delta f_{steady} = -0.05/20 = -0.0025$  p.u. As a result, the support power injected into the grid can be quickly reduced to avoid excessive energy utilization, as shown in Fig. 10 (h). Meanwhile, the support power of MMC1 and MMC3 is approximately proportional to their rated capacities, following equation (22).

In summary, the proposed distributed MPC method achieves the same frequency response as the centralized MPC method. Both OWF kinetic energy and MMC capacitor energy are flexibly utilized and recovered as planned.

### C. Robustness Analysis

#### 1) Successive load disturbances:

To test the performance of the proposed *D-MPC* method under successive load disturbances, two different load disturbances are considered in this case. A 180MW load increase ( $\Delta P_L = 5.6\%$ ) at bus 7 and a 90MW load decrease ( $\Delta P_L = -2.8\%$ ) at bus 9 are applied at  $t=12$ s and  $t=52$ s, respectively. The comparative results of the frequency response using different control methods are depicted in Fig. 11.

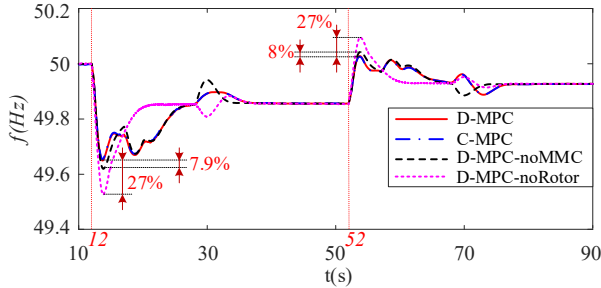


Fig. 11. Comparisons of the frequency responses using different methods.

As can be seen, the *D-MPC* method consistently has the same frequency support performance as the *C-MPC*. Moreover, compared to the *D-MPC-noMMC*, the maximum frequency deviation using the *D-MPC* method is reduced by 7.9% and 8% during the two successive frequency support periods, respectively. In comparison with the *D-MPC-noRotor* method, the reductions are even more significant, reaching 27% in both periods. In addition, the proposed energy recovery strategy also ensures that the maximum frequency deviation during energy recovery is no more than the first frequency deviation.

The control performances of the proposed *D-MPC* method are shown in Fig. 12. Fig. 12 (a) presents the estimated load disturbance power by different distributed MPCs. It can be seen that all MPCs can precisely estimate the two load disturbance powers, which are 5.6% and -2.8%, respectively. Control references and the actual values of the OWF rotor speed and MMC capacitor energy are shown in Fig. 12 (b)-(d). The rotor speed and capacitor energy can follow their references precisely. Meanwhile, the capacitor energy of all MMCs is also utilized consistently. Therefore, the energy coordination capability of

the proposed method is still valid even under two successive load disturbances.

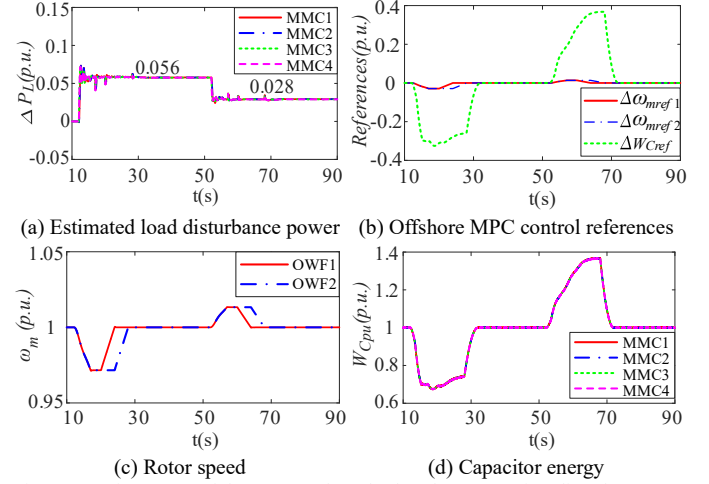


Fig. 12. Performance of the proposed method under successive disturbances.

#### 2) Wind speed variations:

Changing the wind speed of OWF1 from 10.8m/s to 10.3m/s at  $t=12$ s, the performances of the proposed distributed method are shown in Fig. 13. Fig. 13 (a) compares the frequency responses of three different control methods. The proposed *D-MPC* method has the same frequency support effect as the *C-MPC* method and improves the frequency nadir by 10% through the utilization of MMC capacitor energy, and by 26% through the utilization of rotor kinetic energy. Meanwhile, there is no severe frequency drop during energy recovery.

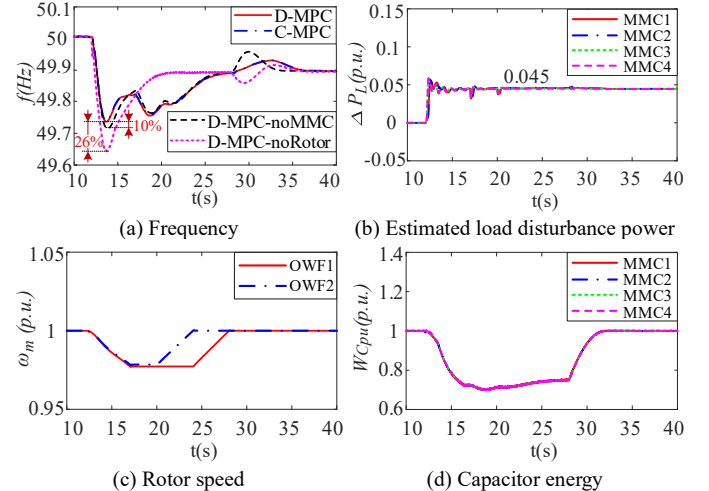


Fig. 13. Performance of the proposed method under wind speed variation.

Fig. 13 (b) shows the estimated power shortage caused by the wind speed change of OWF1, about 4.5%. On this basis, coordinated energy utilization and recovery are also achieved as expected, as shown in Fig. 13 (c) and (d). In summary, the proposed method is still effective in energy coordination and frequency support under wind speed change.

#### 3) Communication time delays:

According to Fig. 4, satellite communication is employed in the proposed *D-MPC* method to sense OWF wind speeds. To test the robustness of the proposed method to communication time delays, two delays of 200ms and 500ms are considered during frequency support. At  $t=12$ s, a 180MW load increase is

applied at bus 7. Wind speeds of both OWFs are set to 10.8m/s. To imitate the communication delays process, the wind speed information in the communication system is initially 0m/s at  $t=12s$ , then updated to 10.8m/s after delays. As a comparison, the same time delays are also applied when using the *C-MPC* method.

Fig. 14 (a) and (b) depict the frequency responses under the two methods. As can be seen, since control references are communicated when using the *C-MPC* method, time delays in control references will cause energy utilization errors and affect the frequency support effect, as shown in Fig. 14 (a). However, in Fig. 14 (b), the proposed *D-MPC* method shows robustness against different time delays in communication. That is because for offshore MMCs, the rotor speed control reference of the connected OWF is generated using the estimated wind speed, independent of communications. As a result, time delays in wind speeds will not affect the rotor speed regulation in OWFs, as shown in Fig. 14 (c) and (d).

Although the time delays in communicating wind speeds may cause an error in MPC constraint (15), the delay duration is much smaller than the time required for the rotor speed to reach its limit (up to the second level). Therefore, the safe utilization of the rotor kinetic energy can still be guaranteed.

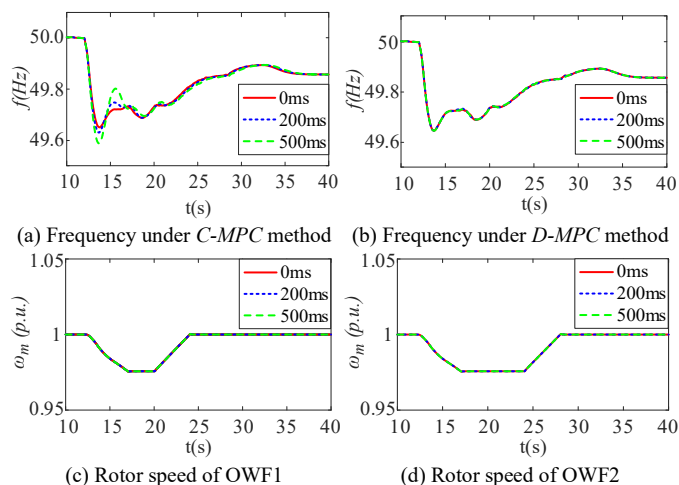


Fig. 14. Performance of the proposed method under communication delays.

## VI. CONCLUSION

For OWFs-MTDC systems, this paper proposes a hierarchical energy control framework that utilizes OWF kinetic energy and MMC capacitor energy to optimize grid frequency response. At the upper-layer, the distributed MPC based energy utilization method is developed to optimally dispatch kinetic and capacitor energies. At the lower-layer, an energy coordination control scheme is designed to enhance energy utilization for frequency support, even without extra power reserves.

Simulation results shows that the designed estimators in distributed MPC controller can precisely calculate the grid frequency, load disturbance power, and wind speed. Thus, it causes that the proposed distributed MPC method has the same frequency support effect as the centralized method. Meanwhile, the proposed energy coordination control can reduce frequency deviations by at least 8%. Moreover, the designed energy

recovery strategy ensures that the frequency deviations during the energy recovery are less than the first deviation.

Robustness analysis demonstrates that under two successive load disturbances and wind speed variations, the proposed method is still available to improve the frequency support effect by coordinating multiple energies. Moreover, communication time delays do not affect the frequency support performance of the proposed distributed method.

Although the proposed MPC-based method has demonstrated good performance in this study, future work will focus on further optimizing MPC parameters to improve adaptability and control effectiveness under varying operating conditions.

## VII. APPENDIX

TABLE A I  
MECHANICAL PARAMETERS OF WIND TURBINE

Parameters	Symbol	Value
Rated wind speed/ $m \cdot s^{-1}$	$w_s$	10.8
Rated rotor speed/p.u.	$\omega_m$	1.0
Air density/ $kg \cdot m^{-3}$	$\rho$	1.225
Inertia time constant/s	$T_j$	4
turbine blade radius /m	$r$	63
Number of pole-pairs	$N_p$	60

TABLE A II  
BASIC PARAMETERS OF MMCs

Parameters	MMC1	MMC3	MMC2, MMC4
Rated capacity/MVA	1400	800	1100
Rated DC voltage/kV	$\pm 400$	$\pm 400$	$\pm 400$
Number of SM per arm	400	400	400
SM capacitance/mF	12.27	6.54	9.0
Voltage ratio (line-to-line)/kV	230/416.41	230/416.41	230/416.41
Leakage reactance $\mu k/\%$	15	15	15

TABLE A III  
BASIC PARAMETERS OF SYNCHRONOUS GENERATORS

	Capacity /MW	Inertia constant /s	Terminal voltage /kV	Transformer ratio
G1~G4	800	3.2	13.8	13.8/230

TABLE A IV  
CONTROL PARAMETERS OF SYNCHRONOUS GENERATORS

Elements	Parameters	Symbol	Value
Governor	Inverse of droop /p.u.	$R$	-20
	Speed relay time constant /s	$T_1$	0.1
	Servo-motor time constant /s	$T_2$	0.3
Turbine	Steam chest time constant /s	$T_3$	0.3
	Reheater time constant /s	$T_4$	10
	Cross-over constant /s	$T_5$	0.4
	$K_3$ fraction /p.u.	$K_3$	0.3
	$K_4$ fraction /p.u.	$K_4$	0.4
	$K_5$ fraction /p.u.	$K_5$	0.3

## VIII. REFERENCES

- [1] W. Xiang, R. Tu, M. Han and J. Wen, "Hybrid AC/DC Collection and HVDC Transmission Topology for Large-scale Offshore Wind Farms," *CSEE J. Power & Energy Syst.*, vol. 11, no. 3, pp. 949-959, May 2025.
- [2] Y. Zhu, Z. Wang and B. Li, "Coordinated Grid-Forming Control Strategy for VSC-HVDC Integrating Offshore Wind Farms Based on Hybrid Energy," *IEEE J. Emerg. Sel. Topics Ind. Electron.*, vol. 5, no. 4, pp. 1350-1361, Oct. 2024.
- [3] W. Xiang, M. Yang and J. Wen, "DR-MMC Hub Based Hybrid AC/DC Collection and HVDC Transmission System for Large-Scale Offshore Wind Farms," *J. Mod. Power Syst. Clean Energy*, vol. 13, no. 2, pp. 452-461, Mar. 2025.

- [4] Y. Wang, W. Xiang, H. Zhang, et al., "Optimal Allocation of Grid-forming and Grid-following WTGs for Stable Weak Grid Integration," *CSEE J. Power & Energy Syst.*, early access, to be published.
- [5] J. Zhu, Z. Shen, S. Bu, et al., "Coordinated flexible damping mechanism with inertia emulation capability for MMC-MTDC transmission systems," *IEEE J. Emerg. Sel. Topics Power Electron.*, vol. 9, no. 6, pp. 7329-7342, Dec. 2021.
- [6] R. Yang, G. Shi, X. Cai, C. Zhang, G. Li and J. Liang, "Autonomous Synchronizing and Frequency Response Control of Multi-terminal DC Systems With Wind Farm Integration," *IEEE Trans. Sustain. Energy*, vol. 11, no. 4, pp. 2504-2514, Oct. 2020.
- [7] H. Liu and C. Liu, "Frequency Regulation of VSC-MTDC System with Offshore Wind Farms," *J. Mod. Power Syst. Clean Energy*, vol. 12, no. 1, pp. 275-286, January 2024.
- [8] Y.-K. Wu, W. H. Yang, Y. L. Hu, et al., "Frequency regulation at a wind farm using time-varying inertia and droop controls," *IEEE Trans. Ind. Appl.*, vol. 55, no. 1, pp. 213-224, Jan./Feb. 2019.
- [9] Y. Xiong, W. Yao, S. Lin, et al., "Improved Communication-Free Coordinated Control of VSC-MTDC Integrated Offshore Wind Farms for Onshore System Frequency Support," *IEEE Trans. Power Del.*, vol. 40, no. 2, pp. 667-680, April 2025.
- [10] L. Liu, X. Luo, L. Xiong, et al., "Preset Power Based Droop Control for Improving Primary Frequency Regulation of Inverters Under Large Disturbances," *IEEE Trans. Power Electron.*, vol. 40, no. 7, pp. 9153-9166, July 2025.
- [11] M. Mehrabankhomartash, M. Saeedifard and A. Yazdani, "Adjustable Wind Farm Frequency Support Through Multi-Terminal HVDC Grids," *IEEE Trans. Sustain. Energy*, vol. 12, no. 2, pp. 1461-1472, Apr. 2021.
- [12] J. Huang, Z. Yang, J. Yu, et al., "Optimization for DFIG Fast Frequency Response With Small-Signal Stability Constraint," *IEEE Trans. Energy Convers.*, vol. 36, no. 3, pp. 2452-2462, Sept. 2021.
- [13] H. Zhang, W. Xiang and J. Wen, "Dual grid-forming control with energy regulation capability of MMC-HVDC system integrating offshore wind farms and weak grids," *IEEE Tran. Power Syst.*, vol. 39, no. 1, pp. 261-272, Jan. 2024.
- [14] S. Yang, J. Fang, Y. Tang, et al., "Modular multilevel converter synthetic inertia-based frequency support for medium-voltage microgrids," *IEEE Trans. Ind. Electron.*, vol. 66, no. 11, pp. 8992-9002, Nov. 2019.
- [15] H. Kim, J. Kang, J. W. Shim, et al., "Exploiting redundant energy of MMC-HVDC to enhance frequency response of low inertia AC grid," *IEEE Access*, vol. 7, pp. 138485-138494, 2019.
- [16] H. Zhang, W. Xiang, Y. He, et al., "Optimal energy utilization of MMC-HVDC system integrating offshore wind farms for onshore weak grid inertia support," *IEEE Trans. Power Syst.*, vol. 39, no. 1, pp. 1304-1318, Jan. 2024.
- [17] M. M. Kabsha and Z. H. Rather, "Adaptive Control Strategy for Frequency Support From MTDC Connected Offshore Wind Power Plants," *IEEE Trans. Power Electron.*, vol. 38, no. 3, pp. 3981-3991, Mar. 2023.
- [18] J. S. Kim, Y. J. Kim and O. Gomis-Bellmunt, "Optimal Frequency Regulation of Multi-Terminal HVDC-Linked Grids With Deloaded Offshore Wind Farms Control," *IEEE Trans. Sustain. Energy*, vol. 15, no. 1, pp. 290-303, Jan. 2024.
- [19] O. Stanojev, U. Markovic, P. Aristidou, G. Hug, D. Callaway and E. Vrettos, "MPC-Based Fast Frequency Control of Voltage Source Converters in Low-Inertia Power Systems," *IEEE Trans. Power Syst.*, vol. 37, no. 4, pp. 3209-3220, July 2022.
- [20] L. Papangelis, M. S. Debry, T. Prevost, et al., "Decentralized model predictive control of voltage source converters for AC frequency containment," *Int. J. Elect. Power Energy Syst.*, vol. 98, pp. 342-349, Jun. 2018.
- [21] S. G. Vennelaganti and N. R. Chaudhuri, "Selective Power Routing in MTDC Grids for Inertial and Primary Frequency Support," *IEEE Trans. Power Syst.*, vol. 33, no. 6, pp. 7020-7030, Nov. 2018.
- [22] P. Mc Namara, R. R. Negenborn, B. De Schutter, et al., "Optimal Coordination of a Multiple HVDC Link System Using Centralized and Distributed Control," *IEEE Trans. Control Syst. Technol.*, vol. 21, no. 2, pp. 302-314, Mar. 2013.
- [23] M. M. Belhauane, K. Almaksour, L. Papangelis, et al., "Implementation and Validation of a Model Predictive Controller on a Lab-Scale Three-Terminal MTDC Grid," *IEEE Trans. Power Del.*, vol. 37, no. 3, pp. 2209-2219, June 2022.
- [24] Q. Yang, J. Shen, J. Li, et al., "An Improved Adaptive Coordination Control of Wind Integrated Multi-Terminal HVdc System," *IEEE Trans. Power Electron.*, vol. 38, no. 4, pp. 5490-5499, Apr. 2023.
- [25] P. Kou, D. Liang, L. Yu, et al., "Nonlinear Model Predictive Control of Wind Farm for System Frequency Support," *IEEE Trans. Power Syst.*, vol. 34, no. 5, pp. 3547-3561, Sept. 2019.
- [26] D. Cirio, F. Conte, B. Gabriele, et al., "Fast Frequency Regulation From a Wind Farm-BESS Unit by Model Predictive Control: Method and Hardware-in-the-Loop Validation," *IEEE Trans. Sustain. Energy*, vol. 14, no. 4, pp. 2049-2061, Oct. 2023.
- [27] Z. Zhang, P. Kou, Y. Zhang, et al., "Coordinated Predictive Control of Offshore DC Collection Grid and Wind Turbines for Frequency Response: A Scheme Without Secondary Frequency Drop," *IEEE Trans. Sustain. Energy*, vol. 14, no. 3, pp. 1488-1503, July 2023.
- [28] H. Clark, N. W. Miller, and J. J. Sanchez-Gasca, "Modeling of GE wind turbine-generators for grid studies," General Electric International Inc, Schenectady, New York, USA, Tech. Rep., Version 4.5, Apr. 2010.
- [29] X. Lei, D. Povh and O. Rühle, "Industrial approaches for dynamic equivalents of large power systems," 2002 IEEE Power Engineering Society Winter Meeting. Conference Proceedings (Cat. No.02CH37309), New York, NY, USA, 2002, pp. 1036-1042.
- [30] R. Bhaskar, M. L. Crow, E. Ludwig, K. T. Erickson and K. S. Shah, "Nonlinear parameter estimation of excitation systems," *IEEE Trans. Power Syst.*, vol. 15, no. 4, pp. 1225-1231, Nov. 2000.
- [31] H. Zhang, J. Wen, W. Xiang, et al., "Multi-degree-of-freedom control framework for HVDC transmission converters," *CSEE J. Power & Energy Syst.*, early access, to be published.
- [32] Y. Xiong, W. Yao, J. Wen, et al., "Two-Level Combined Control Scheme of VSC-MTDC Integrated Offshore Wind Farms for Onshore System Frequency Support," *IEEE Trans. Power Syst.*, vol. 36, no. 1, pp. 781-792, Jan. 2021.
- [33] X. Luo, J. Wang, J. D. Wojcik, et al., "Review of voltage and frequency grid code specifications for electrical energy storage applications," *Energies*, vol. 11, no. 5, pp. 1070, Apr. 2018.
- [34] National Grid, "Enhanced Frequency Response Seminar," 02 06 2016. [Online]. Available: <https://tinyurl.com/hseso8w>.

## BIOGRAPHIES



**Haobo Zhang** received his B.Eng. and PhD degrees both in electrical engineering from Huazhong University of Science and Technology (HUST), China in 2020 and 2025 respectively. He was a visiting PhD student at the Nanyang Technological University (NTU) from 2023 to 2024. Currently, he is a Research Associate at Cardiff University, UK. His research interests include protection and control of MMC-HVDC and DC grids.



**Wang Xiang** (S'16-M'17-SM'25) received his B.Eng. and PhD degrees both in electrical engineering from Huazhong University of Science and Technology (HUST), China in 2012 and 2017 respectively. He was a visiting PhD student at the University of Aberdeen and the University of Strathclyde in 2014 and 2016 respectively. He was with the University of Strathclyde from 2018 to 2021. Currently, he is a Professor at School of Electrical and Electronics Engineering, Huazhong University of Science and Technology, China. His main research interests include MMC-HVDC, high power DC/DC converters, DC grids and offshore wind power integration.



**Yining Wang** received the B.Eng. degree in electrical engineering and automation from Hunan University (HNU), Changsha, China, in 2022, and she is currently working toward the Ph.D. degree in Huazhong University of Science and Technology (HUST). Her research interests include the grid-forming converter control technology.



**Yan Xu** (S'10-M'13-SM'19) received the B.E. and M.E. degrees in electrical engineering from the South China University of Technology, Guangzhou, China, in 2008 and 2011, respectively, and the Ph.D. degree in electrical engineering from the University of Newcastle, Callaghan NSW, Australia, in 2013. After the postdoctoral training with the University of Sydney Postdoctoral Fellowship, he joined Nanyang Technological University (NTU) with the Nanyang Assistant Professorship. He was an Associate Professor in 2021, and the Cham Tao Soon Professor in

Engineering (an endowed professorship named after the founding president of NTU) in 2024. He is currently the Director with Center for Power Engineering (CPE), and Co-Director with Singapore Power Group-NTU Joint Lab, with NTU. His research interests include power system stability and control, microgrids, and data-analytics for smart grid applications. Dr Xu was the recipient of the Nanyang Research Award (Young Investigator) by NTU, and the Outstanding Engineer Award by IEEE Power & Energy Society (PES) Singapore Chapter. He is an Associate Editor for IEEE TRANSACTIONS on SMART GRID and IEEE TRANSACTIONS on POWER SYSTEMS, Chairman of IEEE PES Singapore Chapter (2021 and 2022), and the General Co-Chair of the 11th IEEE ISGT Asia Conference in 2022.



**Jinyu Wen** (M'10-SM'25) received his B.Eng. and Ph.D. degrees all in electrical engineering from Huazhong University of Science and Technology (HUST), Wuhan, China, in 1992 and 1998, respectively. He was a visiting student from 1996 to 1997 and research fellow from 2002 to 2003 all at the University of Liverpool, UK, and a senior visiting researcher at the University of Texas at Arlington, USA in 2010. From 1998 to 2002 he was a director engineer in XJ Electric Co. Ltd. in China. In 2003 he joined the HUST and now

is a Professor at HUST. His current research interests include renewable energy integration, energy storage application, DC grid, and power system operation and control.